A comparison of monodomain and bidomain propagation models for the human heart

Mark Potse,[1,2] Bruno Dubé,[1,2] Alain Vinet,[1,2] and René Cardinal[1,3]

Abstract— **A bidomain reaction-diffusion model of the human heart was developed and potentials resulting from normal depolarization and repolarization were compared with results from a compatible monodomain model. Comparisons were made for an empty isolated heart and for a heart with fluid-filled ventricles. Both sinus rhythm and ectopic activation were simulated. The model took 2 days on 32 processors to simulate a complete cardiac cycle. Differences between monodomain and bidomain results were very small, even for the extracellular potentials which, for the monodomain model, were computed with a high-resolution forward model. Electrograms computed with monodomain and bidomain models were visually indistinguishable. We conclude that, in the absence of applied currents, propagating action potentials on the scale of a human heart can be studied with a monodomain model.**

In memory of Dr. Ramesh M. Gulrajani (1944–2004)

I. INTRODUCTION

The bidomain model of cardiac tissue represents active tissue on a macroscopic scale by relating membrane ionic current, membrane potential (V_m), and extracellular potential (ϕ_e) [1]. It was originally used to derive *forward models*, which compute extracellular and body-surface potentials from given V_m [2]. Later the bidomain model was also used to link multiple membrane models together to form a *bidomain reaction-diffusion (*R-D*) model* [3].

Because bidomain R-D models have to solve an implicit equation to obtain ϕ_e at every step, their use has long been limited to relatively small models. For human-heart simulations, either fixed velocities and waveforms, or monodomain models were used to keep the problem tractable [4]. A monodomain model cannot always be used, because it does not permit currents in the extracellular domain to influence V_m and ionic currents. This influence obviously has to be taken into account when there are applied currents due to pacing or defibrillation [5]. But even when there are no impressed currents, current flow through the extracellular and extracardiac space may influence V_m [3], [6].

Whole-heart bidomain R-D models for the mouse and the rabbit have recently been reported [7], [5]. These models discretize the rodent heart with less than a million nodes. In contrast, a bidomain model of the human heart requires approximately 50 million nodes. Solving the bidomain equations on such a large grid is difficult and requires the use of supercomputers. It is therefore important to determine if a bidomain model is necessary for propagation in the human heart. Several groups have described methods designed for bidomain human-heart models and tested them on a smaller scale [6], [8], [9]. We created a new model which differs from these because of its ability to simulate a complete cardiac cycle at full resolution. In this study we use our new model to compare conduction velocities and ϕ_e between monodomain and bidomain models. To obtain ϕ_e for the monodomain model we used a forward model that computed ϕ_e from V_m in the same way as the bidomain model.

II. METHODS

The model anatomy was based on CT data of a human heart obtained at autopsy [10]. From these data we made a three-dimensional (3-D) finite-difference (FD) grid with 0.2-mm resolution ($567 \times 501 \times 711$ nodes). The atria were not activated in this study, but were retained in order to allow the simulation of a grounding electrode on the right atrium. Fiber orientation was defined mathematically. Fibers rotated transmurally in accordance with measured data [11] and were aligned with the endocardial and epicardial surfaces (Fig. 1).

Three ventricular cell types were used: epicardial cells in the outer 20 % of the wall, M-cells in the next 30 %, and endocardial cells in the inner 50 % [12]. Ionic currents I_ion were computed with the model of the human ventricular cell membrane formulated by Bernus et al. [13], which accounts for these three cell types. The different cell layers are illustrated in Fig. 1. For sinus rhythm simulation, we mimicked the action of the Purkinje network by stimulating the ventricles at the early activation sites and corresponding times published by Durrer et al. [14].

The bidomain model [1] describes the cardiac tissue as consisting of two co-located syncytia termed the intracellular and extracellular domain, characterized by conductivity tensors G_i and G_e, respectively. A current with surface density I_m flows between the two domains. The intracellular and extracellular potentials ϕ_i and ϕ_e are subject to the *bidomain equations*:

$$\nabla \cdot (G_\mathrm{i} \nabla \phi_\mathrm{i}) = \beta I_\mathrm{m} \quad (1)$$
$$\nabla \cdot (G_\mathrm{e} \nabla \phi_\mathrm{e}) = -\beta I_\mathrm{m} \quad (2)$$

where β is the membrane surface-to-volume ratio. The transmembrane current density I_m consists of a capacitive part, an ionic part $I_\mathrm{ion}(V_\mathrm{m}, t)$ generated by the cell membrane, and an imposed stimulation current density I_s:

$$I_\mathrm{m} = C_\mathrm{m} \frac{\partial V_\mathrm{m}}{\partial t} + I_\mathrm{ion} + I_\mathrm{s} \quad (3)$$

From the [1]Research Center, Hôpital du Sacré-Cœur de Montréal, 5400 Boulevard Gouin Ouest, Montréal (Québec), H4J 1C5 Canada; [2]Institute of Biomedical Engineering, Université de Montréal, PO Box 6128, station Centre-ville, Montréal (Québec) H3C 3J7, Canada; and [3]Faculty of pharmacology, Université de Montréal, PO Box 6128, station Centre-ville, Montréal (Québec) H3C 3J7, Canada; e-mail: mark@potse.nl.
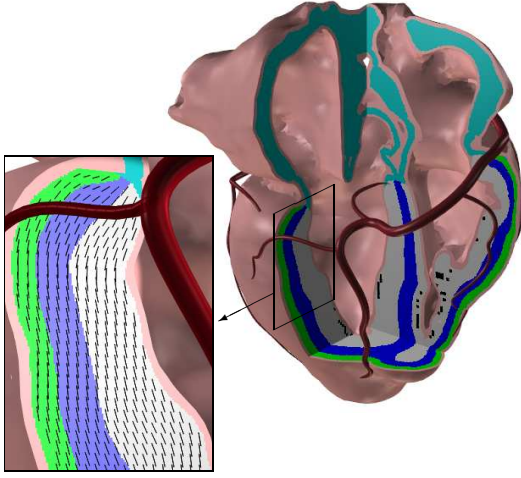
Fig. 1. Top right: heart model showing the tissue embedded in a thin layer of fluid (pink). Tissue types are identified with colors: gray for endocardial, blue for M-cells, green for epicardial, and cyan for connective tissue. Black spots indicate early activation sites, which play the role of Purkinje-muscle junctions in our model. The heart is shown approximately in a posterior view with the left ventricular cavity on the left. Between the atria, the aortic annulus is visible. Coronary arteries are shown for orientation (veins were omitted); most prominent is the right circumflex artery which bends down in the *crux cordis*. Bottom left: detail of the left ventricular wall showing, at 1-mm resolution, the planes in which the fibers lie; the transmural rotation is not shown.

TABLE I
CONDUCTIVITY VALUES (SM^{-1})

material	σ_{eT}	σ_{eL}	σ_{iT}	σ_{iL}
ventricular muscle	0.12	0.30	0.03	0.30
connective tissue	0.20	0.20	0	0
fluid	0.60	0.60	0	0

where C_{m} is the membrane capacitance per unit area. We used $\beta = 1000\,\mathrm{cm}^{-1}$ and $C_{\mathrm{m}} = 1\,\mathrm{\mu F/cm}^2$. Using an operator splitting approach [15] and forward-Euler integration for V_{m} we write the equations in terms of ϕ_{e} and V_{m} as

$$V_{\mathrm{m}}^{t+\delta t} = V_{\mathrm{m}}^t + \frac{\delta t}{\beta C_{\mathrm{m}}}\Big\{ A \cdot (V_{\mathrm{m}}^t + \phi_{\mathrm{e}}^t) - \beta(I_{\mathrm{ion}}^t + I_{\mathrm{s}}^t) \Big\} \quad (4)$$

and

$$B \cdot \phi_{\mathrm{e}}^{t+\delta t} = A \cdot V_{\mathrm{m}}^{t+\delta t} \quad (5)$$

where A and B are $N \times N$ matrices discretizing the operators $\nabla \cdot (G_{\mathrm{e}} + G_{\mathrm{i}})\nabla$ and $\nabla \cdot G_{\mathrm{i}}\nabla$, respectively; N is the number of nodes. G_{e} and G_{i} are inhomogeneous tensor fields. Conductivity values were based on a review of experimental studies by Roth [16]. An overview of all conductivity values in myocardium, fluid, and connective tissue is given in Tab. I. We indicate the conductivities by σ_{eT}, σ_{eL}, σ_{iT}, and σ_{iL} with subscript 'e' for extracellular, 'i' for intracellular, 'T' for transverse, and 'L' for longitudinal.

We computed A and B using an expression proposed by Saleheen and Ng, which accounts for the inhomogeneously anisotropic conductivity and allows discontinuities in the conductivity tensor fields [17]. In their approach, boundaries of the heart are just discontinuities, where $G_{\mathrm{i}} = \underline{0}$ in fluid

and connective tissue and $G_{\mathrm{i}} = G_{\mathrm{e}} = \underline{0}$ in air. The conditions

$$\hat{n} \cdot G_{\mathrm{i}}\nabla\phi_{\mathrm{i}} = 0 \quad \text{on } \partial_{\mathrm{tissue}} \quad (6)$$

$$\hat{n} \cdot G_{\mathrm{e}}\nabla\phi_{\mathrm{e}} = 0 \quad \text{on } \partial_{\mathrm{air}} \quad (7)$$

are satisfied without explicitly enforcing them. In Saleheen and Ng's method [17], the conductivity is constant on "elements" and changes only in a thin transition layer between the elements. An element is a rectangular volume cornered by 8 nodes. Because the conductivity is defined on elements rather than nodes, the boundary is infinitesimally close to the nodes. Nodes on the tissue boundary therefore represent only a part of the tissue volume represented by interior nodes. This was accounted for by assigning them a proportional fraction of the standard value for β.

Equation (5) was solved using a custom-implemented biconjugate gradient stabilized (BICGSTAB) solver [18]. ϕ_{e}^t was used as initial guess for ϕ_{e}^{t+1}. A prediction algorithm based on $V_{\mathrm{m}}^{t+\delta t} - V_{\mathrm{m}}^t$ was used to improve this initial guess. We used an incomplete-LU (ILU) preconditioner, parallelized using domain decomposition [18].

V_{m} was computed with a time step of $\delta t = 10\,\mathrm{\mu s}$. The stepsize was doubled when all cells finished depolarization. As proposed by Vigmond et al., the computation of ϕ_{e} was performed less frequently [15]. We generally updated ϕ_{e} once in every $5\delta t$.

Monodomain simulations were performed by replacing (4) with

$$V_{\mathrm{m}}^{t+\delta t} = V_{\mathrm{m}}^t + \frac{\delta t}{\beta C_{\mathrm{m}}}\Big\{ \nabla \cdot (G'\nabla V_{\mathrm{m}}^t) - \beta(I_{\mathrm{ion}}^t + I_{\mathrm{s}}^t) \Big\} \quad (8)$$

where G' is the "bulk conductivity tensor" [4] whose elements are:

$$G'_{\mu\nu} = \frac{G_{\mathrm{i}\mu\nu} G_{\mathrm{e}\mu\nu}}{G_{\mathrm{i}\mu\nu} + G_{\mathrm{e}\mu\nu}} \quad (9)$$

In both monodomain and bidomain simulations, ϕ_{e} was computed from (5), i.e., based on the bidomain conductivity tensors G_{i} and G_{e}. For the monodomain model, this corresponds to solving a separate forward problem, and is only done once per millisecond of simulated time.

Simulations were performed on 32 processors of an SGI Altix 3700 computer. The program was written in C and parallelized with OpenMP.

III. RESULTS

The heart model at 0.2-mm resolution had 26 million nodes representing active tissue, for which V_{m} and ϕ_{e} were computed, and 10 million nodes representing connective tissue and atrial muscle, for which only ϕ_{e} was computed. Simulations with the resulting 36-million-node "dry heart" model produced $\phi_{\mathrm{e}} > 40\,\mathrm{mV}$ in late-activated areas, which we considered beyond the physiological range [19]. Therefore we performed all following simulations with a 1-mm layer of fluid appended to the endocardial and epicardial surfaces, a situation approximating a Langendorff setup. This measure added 9 million nodes for which ϕ_{e} was computed. Filling the cavities with blood resulted in another 10 million such nodes. Thus, we computed V_{m} at 26 million nodes and
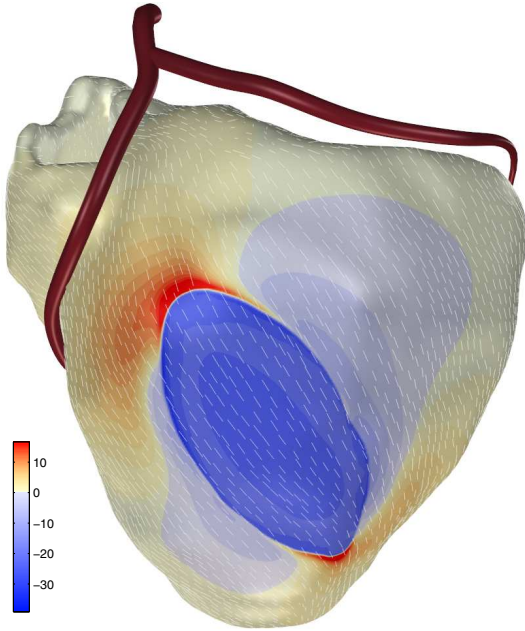
Fig. 2. ϕ_e on the left ventricular epicardial surface 28 ms after subepicardial pacing. Only the ventricular muscle is shown, with the left anterior descending and left circumflex arteries for orientation. Short white line segments indicate epicardial fiber orientation. A nearly elliptic dark-blue area indicates the negative ϕ_e that are due to depolarized tissue; deviations from an elliptic shape are caused by the counterclockwise transmural fiber orientation. Low-level negative ϕ_e also witness this rotation. Positive ϕ_e (yellow to red) occur where depolarization travels along the fibers. The curved positive area, which can be well distinguished on the top left side, is again due to the fact that this longitudinal direction is rotated counterclockwise in deeper layers.

ϕ_e at either 45 million or 55 million nodes. These models used 22 GB and 26 GB of memory, respectively. Simulation of one heart beat (600 ms) in sinus rhythm took 39 hours with empty ventricles and 51 hours with the blood-filled version on 32 processors.

A verification of the model was performed by simulating epicardial potential maps obtained after epicardial and intramural pacing and comparing them to measured data [20]. Development of the potential pattern reflected the transmural rotation of fibers, showing an expansion and counterclockwise rotation of the positive areas for (sub)epicardial pacing, expansion and clockwise rotation for subendocardial pacing, and a more symmetric expansion for mid-wall pacing. The case of sub-epicardial pacing is illustrated in Fig. 2.

To compare monodomain and bidomain models, both sinus rhythm and epicardial pacing experiments were performed. For a sinus beat, total depolarization of the ventricles took 103.5 ms in the monodomain model, 98.4 ms in the dry heart, 97.1 ms in the heart with fluid layer, and 97.0 ms in the heart with filled cavities.

Simulated electrograms are shown in Fig. 3. They demonstrate low-amplitude complexes in the RV basal area, small R waves (initial positive waves) and large S (negative) waves in the middle part of the RV free wall, and large R waves on the left ventricular wall. These features can be observed on the human heart [19]. The figure also shows that differences between monodomain and bidomain models

are small compared to differences between empty and filled ventricles.

Filling of the cavities reduced R-wave amplitude within 4 mm of the endocardial surface by a few millivolts, and increased R-wave amplitude in midmural and epicardial layers by up to 10 mV (Fig. 3). These effects too were accurately reproduced by ϕ_e computed from monodomain V_m. Potentials in the intracavitary fluid were always negative during depolarization, even very close to the endocardium.

IV. DISCUSSION

We have investigated the impact of the monodomain assumption on simulated propagation in an isolated human heart, by comparing results with a bidomain model. Differences between the two models were extremely small, even if ϕ_e was influenced considerably by fluid-filled cavities. There was a small difference in propagation velocity between the two models. All other properties of V_m and ϕ_e were accurately reproduced by the monodomain model with a forward solver for ϕ_e. We have repeated the experiments shown in this paper with simulated ischemia and with the Na conductivity reduced by 90 %, and arrived at the same conclusions.

Since the monodomain approximation is not even approximately valid (Tab. I) it may be expected that monodomain simulation results differ importantly from bidomain results. However, monodomain simulations have provided realistic results. The epicardial potential patterns measured by Taccardi et al. have been reproduced by bidomain, monodomain, and eikonal models [21], [22], [23]. We have demonstrated that even if differences between monodomain and bidomain results can be found, they are small enough to be ignored for most applications, with the obvious exception of those involving applied currents. Another exception must be made with respect to the influence of adjacent fluid on V_m within a few hundred μm from the surface [3]. These effects seem to be ignorable on the scale of a human heart, but they may be significant in smaller hearts, and are critically important for the understanding of superfused preparations [24].

V. ACKNOWLEDGMENT

REFERENCES

[1] C. S. Henriquez, "Simulating the electrical behavior of cardiac tissue using the bidomain model," *CRC Crit. Rev. Biomed. Eng.*, vol. 21, pp. 1–77, 1993.
[2] R. M. Gulrajani and G. E. Mailloux, "A simulation study of the effects of torso inhomogeneities on electrocardiographic potentials, using realistic heart and torso models," *Circ. Res.*, vol. 52, pp. 45–56, 1983.
[3] B. J. Roth, "Action potential propagation in a thick strand of cardiac muscle," *Circ. Res.*, vol. 68, pp. 162–173, 1991.
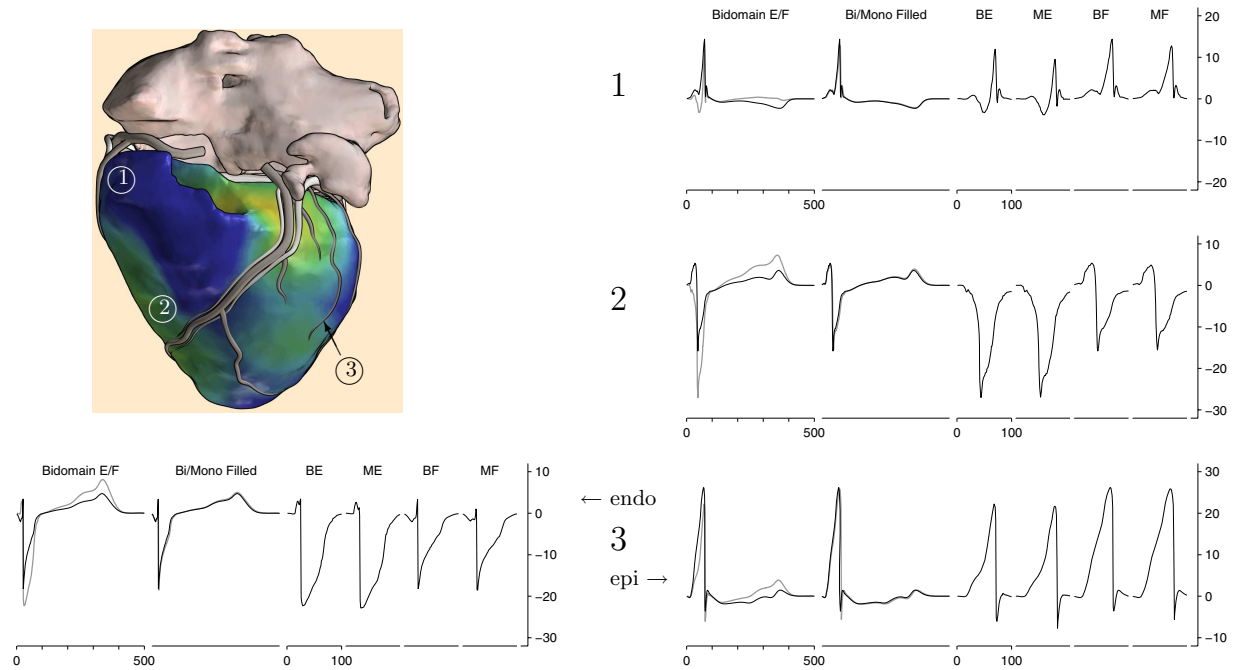
Fig. 3. Examples of ϕ_e traces (electrograms) obtained with a monodomain and forward model and with a bidomain model, at 3 locations on the epicardial surface of the ventricles, and one on the endocardial surface. The 3 epicardial locations are indicated in an anterior view of the heart (connective/fatty tissue omitted), in which activation times are indicated by color (yellow, early to blue, late). Electrograms were obtained either in ventricles with only a fluid layer ("Empty") or with filled cavities ("Filled"). For each site, 6 frames of axes are shown. The first compares empty (gray line) with filled ventricles (black line) in a bidomain simulation. The second frame compares monodomain (gray) with bidomain results (black) for the case of filled ventricles. The remaining four frames show the first 100 ms of the electrogram in empty bidomain (BE); empty monodomain (ME); filled bidomain (BF); and filled monodomain (MF) simulations.

[4] L. J. Leon and B. M. Horáček, "Computer model of excitation and recovery in the anisotropic myocardium. I. Rectangular and cubic arrays of excitable elements," *J. Electrocardiol.*, vol. 24, no. 1, pp. 1–15, 1991.

[5] N. Trayanova and F. Aguel, "Computer simulations of cardiac defibrillation: a look inside the heart," *Comput. Vis. Sci.*, vol. 4, pp. 259–270, 2002.

[6] M. L. Buist and A. J. Pullan, "The effect of torso impedance on epicardial and body surface potentials: A modeling study," *IEEE Trans. Biomed. Eng.*, vol. 50, no. 7, pp. 816–824, 2003.

[7] C. S. Henriquez, J. V. Tranquillo, D. Weinstein, E. W. Hsu, and C. R. Johnson, "Three-dimensional propagation in mathematic models: Integrative model of the mouse heart," in *Cardiac Electrophysiology; From Cell To Bedside*, 4th ed., D. P. Zipes and J. Jalife, Eds. Saunders, 2004.

[8] G. T. Lines, M. L. Buist, P. Grøttum, A. J. Pullan, J. Sundnes, and A. Tveito, "Mathematical models and numerical methods for the forward problem in cardiac electrophysiology," *Comput. Visual. Sci.*, vol. 5, pp. 215–239, 2003.

[9] G. Fischer, B. Tilg, R. Modre, G. J. M. Huiskamp, J. Fetzer, W. Rucker, and P. Wach, "A bidomain model based BEM-FEM coupling formulation for anisotropic cardiac tissue," *Ann. Biomed. Eng.*, vol. 28, pp. 1229–1243, 2000.

[10] M. Lorange and R. M. Gulrajani, "A computer heart model incorporating anisotropic propagation: I. Model construction and simulation of normal activation," *J. Electrocardiol.*, vol. 26, no. 4, pp. 245–261, Oct. 1993.

[11] R. Beyar and S. Sideman, "A computer study of the left ventricular performance based on fiber structure, sarcomere dynamics, and transmural electrical propagation velocity," *Circ. Res.*, vol. 55, pp. 358–375, 1984.

[12] G.-R. Li, J. Feng, L. Yue, and M. Carrier, "Transmural heterogeneity of action potentials and I_{to1} isolated from the human right ventricle," *Am. J. Physiol Heart Circ. Physiol.*, vol. 275, pp. H369–H377, 1998.

[13] O. Bernus, R. Wilders, C. W. Zemlin, H. Verschelde, and A. V. Panfilov, "A computationally efficient electrophysiological model of human ventricular cells," *Am. J. Physiol. Heart Circ. Physiol.*, vol. 282, pp. H2296–H2308, 2002.

[14] D. Durrer, R. T. van Dam, G. E. Freud, M. J. Janse, F. L. Meijler, and R. C. Arzbaecher, "Total excitation of the isolated human heart," *Circulation*, vol. 41, no. 6, pp. 899–912, 1970.

[15] E. J. Vigmond, F. Aguel, and N. A. Trayanova, "Computational techniques for solving the bidomain equations in three dimensions," *IEEE Trans. Biomed. Eng.*, vol. 49, no. 11, pp. 1260–1269, 2002.

[16] B. J. Roth, "Electrical conductivity values used with the bidomain model of cardiac tissue," *IEEE Trans. Biomed. Eng.*, vol. 44, pp. 326–328, 1997.

[17] H. I. Saleheen and K. T. Ng, "New finite difference formulations for general inhomogeneous anisotropic bioelectric problems," *IEEE Trans. Biomed. Eng.*, vol. 44, pp. 800–809, 1997.

[18] Y. Saad, *Iterative Methods for Sparse Linear Systems*. New York: PWS publishing, 1996, second edition published by SIAM, Philadelphia, 2003.

[19] J. P. Roos, R. T. van Dam, and D. Durrer, "Epicardial and intramural excitation of normal heart in six patients 50 years of age and older," *Br. Heart J.*, vol. 30, pp. 630–637, 1968.

[20] B. Taccardi, E. Macchi, R. L. Lux, P. R. Ershler, S. Spaggiari, S. Baruffi, and Y. Vyhmeister, "Effect of myocardial fiber direction on epicardial potentials," *Circulation*, vol. 90, pp. 3076–3090, Dec. 1994.

[21] A. L. Muzikant and C. S. Henriquez, "Paced activation mapping reveals organization of myocardial fibers: A simulation study," *J. Cardiovasc. Electrophysiol.*, vol. 8, pp. 281–294, 1997.

[22] P. Colli-Franzone, L. Guerri, and B. Taccardi, "Modeling ventricular excitation: axial and orthotropic anisotropy effects on wavefronts and potentials," *Math. Biosci.*, vol. 188, pp. 191–205, 2004.

[23] A. E. Pollard, M. J. Burgess, and K. W. Spitzer, "Computer simulations of three-dimensional propagation in ventricular myocardium; effects of intramural fiber rotation and inhomogeneous conductivity on epicardial activation," *Circ. Res.*, vol. 72, no. 744–756, 1993.

[24] B. J. Roth, "Influence of a perfusing bath on the foot of the cardiac action potential," *Circ. Res.*, vol. 86, pp. e19–22, 2000.